Multiple time-scale turbulence model for wall and homogeneous shear flows based on direct numerical simulations

Yasutaka Nagano, Masahide Kondoh and Masaya Shimada
Department of Mechanical Engineering, Nagoya Institute of Technology, Nagoya, Japan

The k–ε model is widely used and has proved effective in predicting wall shear layer turbulence. These models, however, perform poorly in prediction of homogeneous shear flows. Such inconsistency is not caused by crudeness of the eddy-viscosity approximation, but by inappropriate estimation of the relevant time-scale of turbulence. Thus, to settle this problem, we propose a low-Reynolds number-type "multiple time-scale" turbulence model on the basis of recent direct numerical simulations (DNS) of turbulence. Making a proposed model that is applicable to prediction of near-wall turbulent flows without the controversial wall functions and on reproducing the wall-limiting behavior of turbulence quantities is the emphasis. The proposed model has been tested in wall shear flows with and without a pressure gradient. We also tested the present model in homogeneous flows with and without mean strain. Assessments based on the latest DNS data and measurements indicate that the present model works well, regardless of the flow regimes.

Keywords: turbulent flows; turbulence modeling; computational fluid dynamics; multiple scale modeling; low-Reynolds number models; near-wall flow; homogeneous shear flow; homogeneous decaying flow; wall-bounded flow

Introduction

To solve various complicated flows of technological interest, it is now essential to construct a universal, or, more specifically, a multipurpose turbulence model. One of the most basic problems, however, is how to link computations between wall and homogeneous shear flows with a single turbulence model. This has been attempted using the second-order closure model (Abid and Speziale 1993; Hanjalić 1994) or algebraic-stress model (ASM)/nonlinear eddy-viscosity model (Gatski and Speziale 1993; Abe et al. 1997), and reasonable results have been obtained in predicting complex flow domain, although models at this level for both wall and homogeneous flows are still very much a research area. For industrial purposes, the most popular turbulence model is that which employs the eddy-viscosity concept, as represented by the k–ε model. Until now, the k–ε model has been developed mainly for wall-bounded low calculations (Nagano and Tagawa 1990; Myong and Kasagi 1990), and the direct numerical simulation (DNS) data of wall turbulence (Kim 1990; Spalart 1986, 1988) obtained have furthered model prediction accuracy in the vicinity of a wall (Rodi and Mansour 1993; Nagano and Shimada 1993, 1995). However, it is well known that the eddy-viscosity formulation employed in conventional k–ε modeling; i.e., $\nu_t = C_\mu k^2/\varepsilon$, fails in a homogeneous shear flow, and that there is a need to reduce a value of the model constant C_μ empirically to correct predictions (Suzuki et al. 1993). To remove such defects, recent studies have proposed revised k–ε-type turbulence models for homogeneous shear flows. Tzuoo et al. (1986) proposed a zonal-modeling method, in which a flow field is divided into a number of zones, and a final turbulence model is constructed as an assembly of local models optimized in each zone. Yoshizawa and Nishizima (1993) proposed a nonequilibrium k–ε model that gives the effective eddy-viscosity as a function of the Lagrange derivative of turbulent energy and its dissipation rate. These models provided good results in calculating homogeneous shear flows.

On the other hand, Hanjalić et al. (1980) proposed a multiple time-scale (MTS) concept in the eddy–viscosity-type turbulence model. In their modeling, a turbulent energy spectrum was divided into several wave-number (or frequency) regions, and the characteristic time-scale was evaluated independently by the turbulence quantities defined in each region. The eddy-viscosity was estimated by the time-scale of larger (lower wave-number) eddies. Schiestel (1987) further developed the MTS turbulence model on a second-order closure level and discussed the physical meaning of each term in a transport equation valid in each split wave-number region. However, a set of modeled equations becomes so complicated that much effort is needed to make the model actually function. Only lately has the MTS turbulence model using an eddy-viscosity concept similar to Hanjalić et al.

Address reprint requests to Dr. Yasutaka Nagano, Department of Mechanical Engineering, Nagoya Institute of Technology, Gokiso-cho, Showa-ku, Nagoya 466, Japan.

Received 27 March 1995; accepted 25 October 1996

Int. J. Heat and Fluid Flow 18:346–359, 1997

655 Avenue of the Americas, New York, NY 10010

0142-727X/97/$17.00
PII S0142-727X(97)00015-5

(1980) been improved by NASA researchers (Kim and Chen 1989; Kim 1991; Liou 1992; Kim and Benson 1992; Duncan et al. 1993) to analyze complex flows. However, they gave little attention to the near-wall modeling that has developed in recent low-Reynolds number k–ε models. Kim and Chen used the wall functions modified for the MTS model inside the near-wall layer. Kim connected the dissipation rate equation in the MTS model away from a wall to its algebraic formulation in the near-wall region and formed a sort of two-layer MTS model. However, the Kim model reportedly showed differences from the DNS data in predicting most basic fully developed channel flows (Michelassi 1993).

In this paper, we develop a low-Reynolds number MTS model using the eddy-viscosity concept to solve both wall and homogeneous-shear flows. Because near-wall and low-Reynolds number effects are incorporated in the model, the exact wall-limiting behavior of various turbulence quantities is reproduced. Furthermore, the present model is found to provide solutions in good agreement with the DNS data on homogeneous shear flows (Rogers et al. 1986; Matsumoto et al. 1994). We also present the optimum variation in the characteristic time-scale in various wall and homogeneous-shear flows.

Concept of multiple time-scale

The original concept of MTS was proposed by Hanjalić et al. (1980). A sketch of a divided turbulent energy spectrum at large Reynolds numbers is shown in Figure 1. The energy spectrum is split into two wave-number regions; i.e., the production range on the lower side and the transfer range on the upper side. Symbols k_P and k_T in the figure represent the turbulent kinetic energy belonging to each wave-number region, and the sum of these must coincide with the total turbulent kinetic energy k as follows:

$$k_P + k_T = k \tag{1}$$

Inherent to this MTS concept are the restrictions on turbulent production P_k, which affects only the production region, and energy dissipation rate ε_T, which occurs only in the transfer region. The split spectral regions are connected by the energy transfer rate ε_P, which symbolizes the energy cascade mechanism of the turbulent motion.

In the original concept proposed by Hanjalić et al. (1980), the energy spectrum is divided into three regions, and the ε_T is

Notation

C_{f0}	skin-friction coefficient, $C_{f0} = \tau_w/(\rho \bar{U}_0^2/2)$
C_p	static pressure coefficient, $C_p = 2(\bar{P} - \bar{P}_0)/(\rho \bar{U}_0^2)$
$C_{P1}, C_{P2}, C_{T1}, C_{T2}, C_{T3}$	model constants in ε_P- and ε_T-equations
C_μ, C_ν	model constants for eddy-viscosity ν_t
$f_{P1}, f_{P2}, f_{T1}, f_{T2}$	model functions in ε_P- and ε_T-equations
f_t	model function for turbulent diffusion
$f_{r1}, f_{r2}, f_{w1}, f_{w2}$	elements of model functions
f_ν	model function for wall effect
h	channel half-width
K, k	nondimensional acceleration parameter and total turbulent kinetic energy, $K = \nu(d\bar{U}_\infty/dx)/\bar{U}_\infty^2$, $k = \overline{u_i u_i}/2$
k_P	turbulent kinetic energy in lower-wave-number region, $k_P = \int_0^{\kappa'_c} E(\kappa')d\kappa'$
k_T	turbulent kinetic energy in higher-wave-number region, $k_T = \int_{\kappa'_c}^{\kappa'_d} E(\kappa')d\kappa'$
n	exponent coefficient
$\bar{P}, \bar{P}_0$	mean and reference static pressures
P_k	energy production in k_P-equation, $P_k = -\overline{u_i u_j}\,\partial \bar{U}_i/\partial x_j$
Re_τ	Reynolds number, $\mathrm{Re}_\tau = h u_\tau/\nu$
R_t	turbulence Reynolds number, $\mathrm{R}_t = k^2/(\nu\varepsilon_T)$
R_θ	momentum thickness Reynolds number, $\mathrm{R}_\theta = \bar{U}_\infty \theta/\nu$
S	mean shear rate, $S = \partial \bar{U}/\partial y$
t	time
$\bar{U}$	mean velocity component in streamwise direction
$\bar{U}_i, u_i$	mean and fluctuating velocity components in x_i-direction
$\bar{U}_\infty, \bar{U}_0$	free-stream and reference velocities
u_ε	Kolmogorov velocity scale, $u_\varepsilon = (\nu\varepsilon_T)^{1/4}$
u_τ	friction velocity, $u_\tau = \sqrt{\tau_w/\rho}$
x, y, z	streamwise, wall-normal, and spanwise coordinates
y^+, y^*	dimensionless distance from wall, $y^+ = y u_\tau/\nu$, $y^* = y u_\varepsilon/\nu$

Greek

δ_{ij}	Kronecker delta
$\varepsilon, \varepsilon_T$	dissipation rate of k
ε_P	energy transfer rate
η	Kolmogorov length scale, $\eta = (\nu^3/\varepsilon_T)^{1/4}$
θ	momentum thickness
κ, κ'	Kármán constant and wave number
κ'_c, κ'_d	cut-off and Kolmogorov wave numbers
ν, ν_t	kinematic and eddy-viscosities
Π_k, Π_ε	pressure diffusion terms in k_T- and ε_T-equations
ρ	density
$\sigma_k, \sigma_\varepsilon$	model constants for turbulent diffusion
τ_c, τ_k	time-scales, $\tau_c = k_P/\varepsilon_P$, $\tau_k = k/\varepsilon_T$
τ_w	wall shear stress

Subscripts and superscripts

P	production region
T	energy transfer region
w	wall
0	reference and initial points
$\overline{(\ )}$	mean
$(\ )^+$	normalized by wall parameters (u_τ, ν)

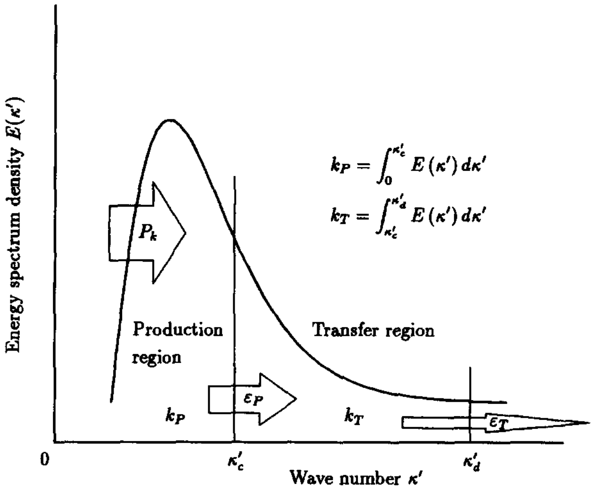

Figure 1 Division of energy spectrum

distinguished from the dissipation rate ε. However, the highest of these three (the dissipation region) has no turbulent energy, because whatever turbulent energy flows into it is immediately dissipated. Hence, the only regions capable of defining the characteristic time- or length-scale are the lower two, where ε_T is substantially equivalent to ε. Kim and Chen (1989) developed their MTS concept on the two-split energy spectrum, and the energy sink of the spectral transfer region ε_T is regarded as the energy dissipation rate. The MTS concept of our investigation, as explained above, followed this simpler idea.

Eddy-viscosity description

The eddy-viscosity formulation employed in the standard k–ε model is

$$\nu_t = C_\mu \frac{k^2}{\varepsilon_T}\left(= C_\mu \frac{k^2}{\varepsilon}\right) \tag{2}$$

where C_μ is a model constant and generally takes the value 0.09. Equation 2 consists of two characteristic turbulence scales; i.e., characteristic velocity scale $\sqrt{k}$ and time-scale k/ε_T. In homogeneous shear flow, however, it is well known that this formulation cannot adequately represent the value of Reynolds stress when experimental data of k and ε_T are substituted in Equation 2 (Tzuoo et al. 1986; Suzuki et al. 1993). This inconsistency is mainly attributable to the inappropriate value of $C_\mu = 0.09$ determined by the equilibrium state of energy production and dissipation in the constant stress layer of wall turbulence. If the value of C_μ is decreased, Equation 2 predicts Reynolds stress correctly in the homogeneous shear flow (Suzuki et al.). This fact indicates that appropriate variations in characteristic time- or length-scale are necessary in analyzing flow fields deviating from the local equilibrium.

Because eddy-viscosity is dominated by large-scale turbulent motions and is not correlated directly with the dissipation rate, it is argued that the dissipation rate ε_T in Equation 2 must be replaced by the energy transfer rate ε_P related to large-scale motions (Kim and Chen 1989; Kim 1991; Liou 1992; Kim and Benson 1992; Duncan et al. 1993):

$$\nu_t = C_\mu \frac{k^2}{\varepsilon_P} \tag{3}$$

In the constant stress layer of wall turbulence, Equation 3 is consistent with Equation 2 because the local equilibrium condition enables $\varepsilon_P = \varepsilon_T$. Under differing flow conditions, however, ε_P can be expected to vary in accordance with deformation in the energy spectrum.

On the other hand, Hanjalić et al. (1980) proposed an eddy-viscosity description using a low wave-number time-scale k_P/ε_P and velocity scale $\sqrt{k}$ as follows:

$$\nu_t = C_\nu \frac{k k_P}{\varepsilon_P} \tag{4}$$

In the present MTS modeling, we employ Equation 4 in the hope of achieving much more flexible performance in ν_t than that obtained from Equation 3 because variable parameters k_P/k and $\varepsilon_P/\varepsilon_T$ are included in Equation 4. As for the model constant C_ν, Hanjalić et al. (1980) adopted $C_\nu = 0.09$, which is identical with the value of C_μ in the standard k–ε model, Equation 2. However, a lower value of ν_t in a log-law region of the wall-bounded flow may be expected, because in this region, $\varepsilon_P = \varepsilon_T$ (as explained above) and $k_P < k$ would seem to follow. Thus, considering the following relation derived from Equation 2 and 4:

$$C_\mu = C_\nu \frac{k_P}{k}\frac{\varepsilon_T}{\varepsilon_P} \tag{5}$$

we take the model constant C_ν as the larger value. Note that, in the proposed MTS model, C_μ becomes a function of k_P/k and $\varepsilon_P/\varepsilon_T$, both of which are expected to reflect the flow condition correctly for the coefficient C_μ that is taken as a constant value in the conventional k–ε model.

Model equations

In view of the physical concept in Figure 1, it is evident that the energy transfer rate ε_P is an energy sink term for the production region, while simultaneously being a source term for the transfer region. Hence, the transport equations for turbulent kinetic energies in each spectral region are given as follows:

$$\frac{Dk_P}{Dt} = \frac{\partial}{\partial x_j}\left[\left(\nu + f_t \frac{\nu_t}{\sigma_k}\right)\frac{\partial k_P}{\partial x_j}\right] + P_k - \varepsilon_P \tag{6}$$

$$\frac{Dk_T}{Dt} = \frac{\partial}{\partial x_j}\left[\left(\nu + f_t \frac{\nu_t}{\sigma_k}\right)\frac{\partial k_T}{\partial x_j}\right] + \varepsilon_P - \varepsilon_T + \Pi_k \tag{7}$$

where $P_k = -\overline{u_i u_j}\,\partial \overline{U}_i/\partial x_j$ is the energy production rate attributable to the mean velocity gradient, and $D/Dt = \partial/\partial t + \overline{U}_j \partial/\partial x_j$ implies the substantial derivative. Turbulent diffusion terms are based on the gradient diffusion model where σ_k is a model constant, and f_t is a model function representing increasing turbulent diffusion in the near-wall region, as observed in DNS data (see Nagano and Shimada 1993, 1995). The symbolized Π_k is a pressure diffusion term of the kinetic energy equation.

The energy transfer ε_P and dissipation rate ε_T equations can be modeled by using the characteristic time-scales k_P/ε_P, and

k_T/ε_T in each of the spectral region as follows:

$$\frac{D\varepsilon_P}{Dt} = \frac{\partial}{\partial x_j}\left[\left(\nu + f_t \frac{\nu_t}{\sigma_\varepsilon}\right)\frac{\partial \varepsilon_P}{\partial x_j}\right] + C_{P1} f_{P1} \frac{P_k \varepsilon_P}{k_P} - C_{P2} f_{p2} \frac{\varepsilon_P^2}{k_P} \tag{8}$$

$$\frac{D\varepsilon_T}{Dt} = \frac{\partial}{\partial x_j}\left[\left(\nu + f_t \frac{\nu_t}{\sigma_\varepsilon}\right)\frac{\partial \varepsilon_T}{\partial x_j}\right] + C_{T1} f_{T1} \frac{\varepsilon_P \varepsilon_T}{k_T} - C_{T2} f_{T2} \frac{\varepsilon_T^2}{k_T} + \Pi_\varepsilon \tag{9}$$

where C_{P1}, C_{P2}, C_{T1}, C_{T2} are models constants, and f_{P1}, f_{P2}, f_{T1}, f_{T2} are model functions representing low-Reynolds number and/or near-wall turbulence. The symbolized Π_ε is a pressure diffusion term of the dissipation-rate equation.

The Reynolds stress formulation can algebraically be expressed as

$$-\overline{u_i u_j} = \nu_t\left(\frac{\partial \overline{U}_i}{\partial x_j} + \frac{\partial \overline{U}_j}{\partial x_i}\right) - \frac{2}{3}\delta_{ij} k \tag{10}$$

and the eddy-viscosity is given from Equation 4 as follows:

$$\nu_t = C_\nu f_\nu \frac{k k_P}{\varepsilon_P} \tag{11}$$

where f_ν denotes a model function representing the wall-proximity effect.

These equation are solved with the mass conservation and momentum conservation equations:

$$\frac{\partial \overline{U}_i}{\partial x_i} = 0 \tag{12}$$

$$\frac{D\overline{U}_i}{Dt} = -\frac{1}{\rho}\frac{\partial \overline{P}}{\partial x_i} + \frac{\partial}{\partial x_j}\left(\nu \frac{\partial \overline{U}_i}{\partial x_j} - \overline{u_i u_j}\right) \tag{13}$$

Determination of model constants

For a fundamental construction of the present MTS model, we must find some physical relation among model constants under basic flow conditions. The constant stress layer (log-law region) of the wall turbulent flow and the homogeneous decaying flow are the best candidates for such a purpose.

In the constant stress layer of the wall turbulent flow, well-known approximation equations are given by

$$P_k \simeq \varepsilon_P \simeq \varepsilon_T \tag{14}$$

$$-\overline{uv} \simeq u_\tau^2 \tag{15}$$

$$\frac{\partial \overline{U}}{\partial y} \simeq \frac{u_\tau}{\kappa y} \tag{16}$$

Here, u_τ is the friction velocity, and κ is the Kármán constant generally taking a value of 0.4 in the fully developed channel flow.

Because the structure parameter $(-\overline{uv}/k)$ takes a value of about 0.3 in this layer, Equation 2 with $C_\mu = 0.09$ gives the correct value of the eddy-viscosity. Hence, from Equation 2, 4 and 14, we have

$$\frac{k_P}{k} = \frac{0.09}{C_\nu} \tag{17}$$

Consequently, k_P/k takes a constant value in the constant stress layer of the wall turbulence.

By substituting Equations 14–16 for the ε_P Equation 8 and the ε_T Equation 9, we deduce the following relations for model constants:

$$\frac{k_P}{k} = \frac{(C_{P2} - C_{P1})^2 \sigma_\varepsilon^2 C_\nu}{\kappa^4} \tag{18}$$

$$\frac{k_T}{k} = \frac{(C_{P2} - C_{P1})(C_{T2} - C_{T1})\sigma_\varepsilon^2 C_\nu}{\kappa^4} \tag{19}$$

From Equations 18, 19, and 1, a combined equation for model constants employed in ε_P Equation 8 and ε_T Equation 9 is derived as follows:

$$(C_{P2} - C_{P1})(C_{P2} - C_{P1} + C_{T2} - C_{T1}) = \frac{\kappa^4}{\sigma_\varepsilon^2 C_\nu} \tag{20}$$

Also, by substituting k_P/k given by Equation 17 for Equation 18, we have the following C_ν equation in the constant stress layer:

$$C_\nu = \frac{\sqrt{0.09}\,\kappa^2}{(C_{P2} - C_{P1})\sigma_\varepsilon} \tag{21}$$

Here, we emphasize that Equations 18, 19, and 21 must be reconciled to adequately predict the constant stress layer.

In the homogeneous decaying turbulence, on the other hand, it is well known from much experimental data that the decay law of turbulent kinetic energy is given by

$$k \,\alpha\, x^{-n} \tag{22}$$

where x is a coordinate of flow direction, and n is an exponent coefficient taking the value $1 \sim 1.25$ in the initial period (Batchelor and Townsend 1948a; Comte-Bellot and Corrsin 1966), and 2.5 in the final period (Corrsin 1951).

The decay law (22) is extended to the divided turbulent energy k_P and k_T as follows (Hanjalić et al. 1980):

$$k_P = A\frac{k_P}{k}x^{-n}, \qquad k_T = A\frac{k_T}{k}x^{-n} \tag{23}$$

where A is a numerical coefficient. It is safe to say that parameters k_P/k and k_T/k take constant values until the final period of decay, because the energy cascade motion of turbulent eddies holds even in the final phase of dissipation (Hanjalić et al. 1980). However, it should be noted that the disappearance of k_P or k_T is thought to eliminate the energy cascade mechanism that is abridged as ε_P in the present MTS model equations.

In the homogeneous decaying turbulent flow, the energy production and diffusion can be ignored entirely, so that the governing equations are written in the following simple forms:

$$\bar{U}\frac{\mathrm{d}k_P}{\mathrm{d}x} = -\varepsilon_P \tag{24}$$

$$\bar{U}\frac{\mathrm{d}\varepsilon_P}{\mathrm{d}x} = -C_{P2}f_{P2}\frac{\varepsilon_P^2}{k_P} \tag{25}$$

$$\bar{U}\frac{\mathrm{d}k_T}{\mathrm{d}x} = \varepsilon_P - \varepsilon_T \tag{26}$$

$$\bar{U}\frac{\mathrm{d}\varepsilon_T}{\mathrm{d}x} = C_{T1}\frac{\varepsilon_P\varepsilon_T}{k_T} - C_{T2}f_{T2}\frac{\varepsilon_T^2}{k_T} \tag{27}$$

Here, we put $f_{T1} = 1$ in conformity with conventional low-Reynolds number k–ε modeling (Nagano and Hishida 1987). Because Equations 24 and 26 with Equation 23 yield the following asymptotic solutions for ε_P and ε_T:

$$\varepsilon_P = A\bar{U}\frac{k_P}{k}nx^{-(n+1)}, \qquad \varepsilon_T = A\bar{U}nx^{-(n+1)} \tag{28}$$

we find that an important relation holds in the homogeneous decaying turbulent flow:

$$\frac{\varepsilon_P}{\varepsilon_T} = \frac{k_P}{k} \tag{29}$$

Having an alternative form $k_P/\varepsilon_P = k/\varepsilon_T$, Equation 29 indicates that the characteristic time-scale for eddy-viscosity in the present MTS model is identical with the time-scale of the standard k–ε model in the homogeneous decaying turbulent flow.

Substituting Equations 23 and 28 for Equations 25 and 27, we have a set of equations as follows:

$$C_{P2}f_{P2} = \frac{n+1}{n} \tag{30}$$

$$(C_{T2}f_{T2} - C_{T1})\frac{k}{k_T} + C_{T1} = \frac{n+1}{n} \tag{31}$$

By using the above set of equations, we can determine model functions f_{P2} and f_{T2} so that they take value unity in the initial period of decay where the exponent coefficient $n = 1.1$ and vary from unity in the final period of decay where $n = 2.5$. The model function f_{P2} is immediately determined from Equation 30; whereas, f_{T2} cannot readily be obtained from Equation 31. Assuming that the ratio k_T/k is constant during the decay, we derive the following relation from Equations 30 and 31:

$$\frac{C_{T2}f_{T2} - C_{T1}}{(n+1)/n - C_{T1}} = \frac{C_{T2} - C_{T1}}{C_{P2} - C_{T1}} \tag{32}$$

which yields a convenient equation for f_{T2}:

$$C_{T2}f_{T2} = \left(\frac{n+1}{n} - C_{T1}\right)\frac{C_{T2} - C_{T1}}{C_{P2} - C_{T1}} + C_{T1} \tag{33}$$

Consequently, the form of f_{T2} can be settled using the predetermined values of model constants C_{T1}, C_{T2}, C_{P2}, and decay exponent n.

For obtaining a complete set of relational equations among model constants that ensure an adequate solution in both the constant stress layer (i.e., wall turbulence) and homogeneous decaying flow (i.e., free turbulence), it is necessary to combine the equations we derived on the condition of both flows. First, we assume that the model function f_{T2} in Equation 31 is equal to unity in the log-law region where the turbulence level is sufficiently high. Then, by substituting Equation 19 for Equation 31 to eliminate k_T/k, we have

$$(C_{P2} - C_{P1})(C_{P2} - C_{T1}) = \frac{\kappa^4}{\sigma_\varepsilon^2 C_\nu} \tag{34}$$

From comparison of Equation 20 with Equation 34, a simple relation is derived:

$$C_{P1} = C_{T2} \tag{35}$$

Also, we have the following relation from Equations 21 and 34:

$$C_{T1} = C_{P2} - \frac{\kappa^2}{\sigma_\varepsilon\sqrt{0.09}} \tag{36}$$

Using the set of Equations 21, 30, 35, and 36 with numerical optimization on the fully developed channel flow and the homogeneous shear flow, we determine model constants as follows:

$$\begin{aligned} &C_\nu = 0.14, \quad \sigma_k = 1.0, \quad \sigma_\varepsilon = 1.4, \\ &C_{P1} = 1.65, \quad C_{P2} = 1.9, \quad C_{T1} = 1.5, \quad C_{T2} = 1.65 \end{aligned} \tag{37}$$

On the other hand, from Equations 30 and 33, the model functions f_{P2} and f_{T2} are given by:

$$f_{P2} = 1 - 0.3f_{r2} \tag{38}$$

$$f_{T2} = 1 - 0.13f_{r2} \tag{39}$$

where $R_t = k^2/(\nu\varepsilon_T)$ is the turbulence Reynolds number and $f_{r2} = \exp[-(R_t/12.5)^{1/2}]$ is one of the element functions to be defined later. The forms of Equations 38 and 39 are determined with reference to the model function in the k–ε model proposed by Coleman and Mansour (1993). Determining f_{P2} and f_{T2} as above, the decay low (Equation 23) is held all over the period of decay. Again, note that f_{P1} and f_{T1} are unity, both in the constant stress layer of wall turbulent flow and the homogeneous shear flow in the calculations shown in the Results and discussion section.

Modeling near-wall turbulence

For application of the turbulence model to calculate heat transfer from the solid wall, it is important that the model represents near-wall behavior of the turbulence quantities (Myong et al. 1989; Youssef et al. 1992). In the vicinity of the wall, the molecular viscosity effect is superior to the turbulent mixing, and a strong anisotropic condition holds. In the present MTS modeling, to represent these wall-proximity effects adequately, we introduce the following set of functions as an element of model functions:

$$f_{w1} = \exp[-(y^*/20)^2] \tag{40}$$

$$f_{w2} = \exp[-(y^*/3.3)^2] \tag{41}$$

$$f_{r1} = \exp[-(R_t/80)^2] \tag{42}$$

$$f_{r2} = \exp[-(R_t/12.5)^{1/2}] \tag{43}$$

where ($y^* = yu_\varepsilon/\nu$, which was first introduced by Abe et al. (1994) in the k–ε model, denotes a nondimensional distance from the wall using the Kolmogorov velocity scale $u_\varepsilon = (\nu\varepsilon_T)^{1/4}$.

Note that $u_\varepsilon > 0$ is always assured in every turbulent flow. Hence y^* is considered more suitable than $y^+ = u_\tau y/\nu$, which is most widely used in low-Reynolds number k–ε models, for computing complicated turbulent flows with separation or reattachment where the friction velocity u_τ is always zero. There may be a situation where appropriate definition of the unique wall distance y is impossible in complex flow geometries. To avoid such a problem, it is hoped that the model function is formulated without the wall distance y. However, we have not found an alternative parameter to y that is sufficient in both accuracy and simplicity. We are continuing efforts to develop a new wall parameter alternative to y.

Next, we consider wall-limiting behavior of various turbulence quantities used in the present MTS model. Near-wall behavior of the total turbulent kinetic energy k and its dissipation rate ε_T is represented as expansions of powers around $y = 0$ (Chapman and Kuhn 1986):

$$k = ay^2 + by^3 + O(y^4) \tag{44}$$

$$\varepsilon_T(=\varepsilon) = 2\nu a + 4\nu by + O(y^2) \tag{45}$$

where the coefficients a, b, etc. are functions of x and z alone.

In the same way, the near-wall expansions of k_P and k_T are given by assuming k_P/k and k_T/k as constants (or $k_P/k_T =$ const) in a narrow region in the vicinity of the wall as follows:

$$k_P = \frac{k_P}{k}[ay^2 + by^3 + O(y^4)] \tag{46}$$

$$k_T = \frac{k_T}{k}[ay^2 + by^3 + O(y^4)] \tag{47}$$

Hence, the wall-limiting behavior of $k_P \propto y^2$ and $k_T \propto y^2$ is maintained. Note that Equation 44 exactly leads to Equations 46 and 47. The assumption that $k_P/k_T =$ const very near the wall is originated from the following arguments. First, very near the wall, turbulent energy must change montonously in y-direction because of the negligible turbulent production. Hence, if we assume the ratio k_P/k_T is variable, the alternative low- or high-wave number energy may quickly vanish as the wall is approached, and ε_P becomes nearly zero. This means the vanish of the energy cascade according to the MTS concept, which is illegitimate.

The energy-transfer rate Equation 6 is deduced in the near-wall region as:

$$\nu\frac{\partial^2 k_P}{\partial y^2} - \varepsilon_P = 0 \tag{48}$$

By substituting Equation 46 for Equation 48, we have the near-wall expansion of ε_P:

$$\varepsilon_P = \frac{k_P}{k}[2\nu a + 6\nu by + O(y^2)] \tag{49}$$

From Equations 46 and 49, we have the wall boundary condition of ε_P as follows:

$$\varepsilon_{Pw} = 2\nu\left(\frac{\partial\sqrt{k_P}}{\partial y}\right)^2_w \tag{50}$$

On the other hand, the k_T Equation (7) in the near-wall region is given as follows:

$$\nu\frac{\partial^2 k_T}{\partial y^2} + \varepsilon_P - \varepsilon_T + \Pi_k = 0 \tag{51}$$

With Equations 47, 49, and 1, we have the expansion equation from Equation 51:

$$\varepsilon_T = 2\nu a + 6\nu by + O(y^2) + \Pi_k \tag{52}$$

From a comparison of Equations 45 and 52, Π_k must have the near-wall behavior $-2\nu by$ to balance the k_T equation in the vicinity of the wall. Therefore, referring to Nagano and Shimada's (1993, 1995), k–ε model, we model the pressure diffusion terms Π_k and Π_ε as follows:

$$\Pi_k - \frac{1}{2}\nu\frac{\partial}{\partial x_j}\left(\frac{k}{\varepsilon_T}\frac{\partial\varepsilon_T}{\partial x_j}f_{w2}\right) \tag{53}$$

$$\Pi_\varepsilon = C_{T3}\nu\frac{\partial}{\partial x_j}\left[(1-f_{w2})\frac{\varepsilon_T}{k}\frac{\partial k}{\partial x_j}f_{w2}\right] \tag{54}$$

where C_{T3} is a model constant and determined as 0.5. The pressure diffusion term Π_ε (Equation 54) has the wall-limiting behavior $\Pi_\varepsilon \propto y^0$, which is in agreement with the DNS. From Equations 44 and 45, the boundary condition of the dissipation rate ε_T at the wall is determined as follows:

$$\varepsilon_{Tw} = 2\nu\left(\frac{\partial\sqrt{k}}{\partial y}\right)^2_w \tag{55}$$

Equation 55 coincides with the boundary condition employed in the conventional near-wall k–ε models (Nagano and Tagawa 1990; Myong and Kasagi 1990; Nagano and Shimada 1993, 1995). Equations 49 and 45 show that the following relation between ε_P and ε_T holds in the vicinity of the wall:

$$\frac{\varepsilon_P}{\varepsilon_T} = \frac{k_P}{k} \tag{56}$$

This relation is exactly the same as Equation 29 in the homogeneous decaying flow, and there seems to be a common situation of zero turbulent production. Equation (56) indicates that the characteristic time-scale describing eddy-viscosity in the present MTS model is now identical with the time-scale of the k–ε model near the wall. Provided that the situation in Equation 56 holds, the formulation of the eddy-viscosity becomes

$$\nu_t = C_\nu f_\nu\frac{kk_P}{\varepsilon_P} = C_\nu f_\nu\frac{k^2}{\varepsilon_T} \tag{57}$$

Hence, the eddy-viscosity formulation near the wall is identical with that in the k–ε model and, consequently, the form of model function f_ν can be analogized to that employed in a conventional low-Reynolds number k–ε model. Near the wall, $\nu_t \propto y^3$ holds, and Equations 44, 45, and 57 require near-wall behavior $f_\nu \propto y^{-1}$.

We employed the following form of f_ν to satisfy this wall-limiting behavior:

$$f_\nu = (1 - f_{w1})(1 + 14R_t^{-3/4} f_{r1}) \tag{58}$$

where the first half of the right-hand side is the Van Driest-type dumping function, the second half has the role of adjusting the length scale of eddy-viscosity in the vicinity of the wall, and f_{r1} ensures that $f_\nu = 1$ far from the wall. From Equations 57 and 58, the eddy-viscosity formulation in the vicinity of the wall is deduced as follows:

$$\nu_t \propto y^{*2} \frac{k^2}{\varepsilon_T} R_t^{-3/4} = y^2 k^{1/2}/\eta (\propto y^3) \tag{59}$$

where $\eta = (\nu^3/\varepsilon_T)^{1/4}$ is the Kolmogorov length scale. Equation 59 indicates that the dissipation process governs turbulent motion very near the solid surface.

From a consideration of the wall-limiting behavior of the source and sink terms of Equations 8 and 9, the following model functions are proposed to avoid the divergence of equations near the wall:

$$f_{P1} = 1 \tag{60}$$

$$f_{P2} = (1 - f_{w2})(1 - 0.3 f_{r2}) \tag{61}$$

$$f_{T1} = 1 - f_{w2} \tag{62}$$

$$f_{T2} = (1 - f_{w2})(1 - 0.13 f_{r2}) \tag{63}$$

Note that f_{P2} and f_{T2} contain model functions 38 and 39, respectively, to represent asymptotic behavior of turbulence quantities in the homogeneous decaying turbulence.

It is now established from DNS data that the turbulent diffusion term increases in the vicinity of wall (e.g., see Cazalbou and Bradshaw 1993). However, a standard gradient diffusion-type model is less likely to predict this profile. To solve such a discrepancy, Nagano and Shimada (1993, 1995) proposed an additional model function f_t with the turbulent diffusion term of k and ε equations. Adopting this result into the present MTS model, the following model function is introduced into the turbulent diffusion term of each transport equation.

$$f_t = 1 + 3.5 f_{r1} \tag{64}$$

Results and discussion

Homogeneous decaying flow

First to check the fundamental performance of the model Equations 6–9, we apply the present model to the homogeneous decaying flow. The deduced transport equations are given as Equations 24–27. Because these are ordinary differential equations, we choose the 4th order Runge–Kutta method for solving them.

From relation 29, the characteristic time-scale k_P/ε_P is identical with the time-scale of k–ε model; i.e., k/ε_T. Hence, the profile of the dissipation rate obtained by solving Equation 27 should be identical with the solution of the ε equation of the k–ε model, that is:

$$\bar{U} \frac{d\varepsilon_T}{dx} = -C_{\varepsilon 2} f_\varepsilon \frac{\varepsilon_T^2}{k} \tag{65}$$

where $C_{\varepsilon 2}$ is a widely used model constant with a value of 1.9, and f_ε is a model function equal to one at the initial period.

From Equations 27 and 65, we derive

$$\frac{k_P}{k} = \frac{C_{\varepsilon 2} f_\varepsilon - C_{T2} f_{T2}}{C_{\varepsilon 2} f_\varepsilon - C_{T1}} \tag{66}$$

At the initial period of decay, because all model functions in Equation 66 take value unity, we have an initial condition of k_P/k from Equation 66. Furthermore, the initial value of ε_P is obtained by substituting Equation 66 for Equation 29.

Figure 2 shows the decay of turbulent energy k and its dissipation rate ε_T, as compared with the DNS data of Iida and Kasagi (1993). For the initial conditions of each turbulence quantity, we use the DNS data at $t = 2$, at which the energy spectrum is well developed. The present model represents the asymptotic profiles of the initial period of decay; i.e., $k \propto t^{-1.1}$ and $\varepsilon_T \propto t^{-2.1}$, and the agreement with the DNS data is almost complete.

Furthermore, we continue the calculation downstream and compare the turbulence Reynolds number profile with the experimental data of Batchelor and Townsend (1948a, b) in the intermediate period of decay. As shown in Figure 3, the present model predicts well the experimental data both of $\mathrm{Re}_M = 650$ and 1360. From the results presented in this subsection, it is concluded that the present MTS model predicts the homogeneous decaying flow accurately.

Homogeneous shear flow

In this subsection, we explain the validity of the present MTS model, especially, in analyzing homogeneous turbulent shear flow. To determine the initial condition of k_P/k and ε_P using available k, ε_T and $-\overline{uv}$ data from the experiment or DNS data, we employ the asymptotic relation proposed by Kim and Benson (1992) in the homogeneous flow and under an equilibrium condition where P_k/ε_T is nearly constant:

$$\frac{k_P}{k_T} = \frac{Dk_P}{Dk_T} = \frac{P_k - \varepsilon_P}{\varepsilon_P - \varepsilon_T} \tag{67}$$

From Equations 1, 4 and 67, we have the initial value of the ratio k_P/k as follows:

$$\frac{k_P}{k} = \frac{P_k}{P_k - \varepsilon_T - C_\nu (k^2/\overline{uv}) S} \tag{68}$$

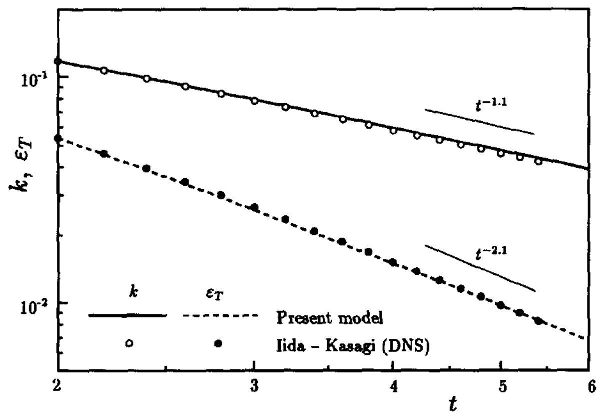

Figure 2 Profiles of turbulent energy and dissipation rate during the initial period of decay (Iida and Kasagi 1993)

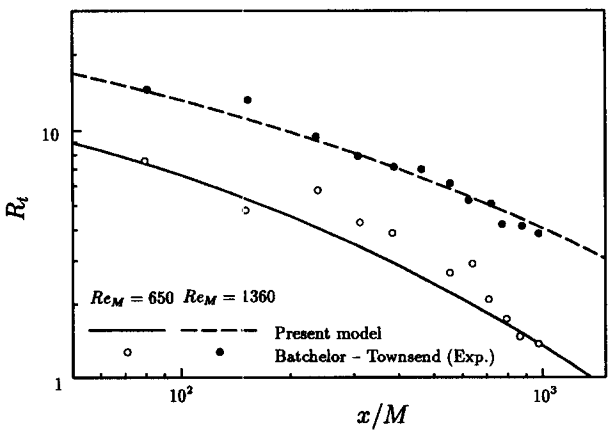

Figure 3 Profile of turbulence Reynolds number in intermediate period (Batchelor and Townsend 1948a, b)

where S is the mean shear rate, and the initial value of ε_P is obtained from Equations 68 and 4.

The only difference between the transport equations of the homogeneous shear flow and those used in the homogeneous decaying flow is the existence of a turbulent production term. Hence, the fourth-order Runge–Kutta method is once again employed as the calculation method.

For comparison, we calculate conventional and recent turbulence models using the eddy-viscosity concept as follows: standard-type k–ε model; nonequilibrium k–ε model proposed by Yoshizawa and Nishizima (1993); zonal model for the homogeneous shear flow proposed by Tzuoo et al. (1986); and MTS model proposed by Duncan et al. (1993). These models are solved by the same numerical method as the present model.

Calculations of these models are carried out under conditions derived from three DNS data, as shown in Table 1: C128W and C128U simulation data given by Rogers et al. (1986), and CASE2 simulation data presented by Matsumoto et al. (1994). Initial values of $k_P/k, k_T/k$, and $\varepsilon_P/\varepsilon_T$ from Equations 68 and 4 are: $k_{P0}/k_0 = 0.509$, $k_{T0}/k_0 = 0.491$, $\varepsilon_{P0}/\varepsilon_{T0} = 1.29$ (C128W); $k_{P0}/k_0 = 0.638$, $k_{T0}/k_0 = 0.362$, $\varepsilon_{P0}/\varepsilon_{T0} = 1.17$ (C128U); $k_{P0}/k_0 = 0.492$, $k_{T0}/k_0 = 0.508$, $\varepsilon_{P0}/\varepsilon_{T0} = 3.10$ (CASE2).

Figure 4 shows the calculation results on the condition of C128W presented by Rogers et al. (1986). It appears that the standard k–ε model predicts each quality as too great, and the nonequilibrium k–ε model underestimates the time evolution of turbulence. However, the present and zonal k–ε models predict DNS data quite well. In this flow condition, the recent MTS model proposed by Duncan et al. (1993) does not work at all

Table 1 Initial conditions of calculation in homogeneous shear flows

	C128W [DNS: Rogers et al. (1986)]	C128U [DNS: Rogers et al. (1986))	CASE2 [DNS: Matsumoto et al. (1994)]
ν	0.02	0.01	7.692×10^{-3}
S	56.568	28.284	$10\sqrt{2}$
St_0	12.0	8.0	2.0
k_0	1.47×10^1	6.38	2.52×10^{-1}
ε_{T0}	1.55×10^2	4.10×10^1	2.34×10^{-1}
$-\overline{uv}_0$	4.36	2.14	8.52×10^{-2}
k_{P0}/k_0	0.509	0.638	0.492
k_{T0}/k_0	0.491	0.362	0.508
$\varepsilon_{P0}/\varepsilon_{T0}$	1.29	1.17	3.10

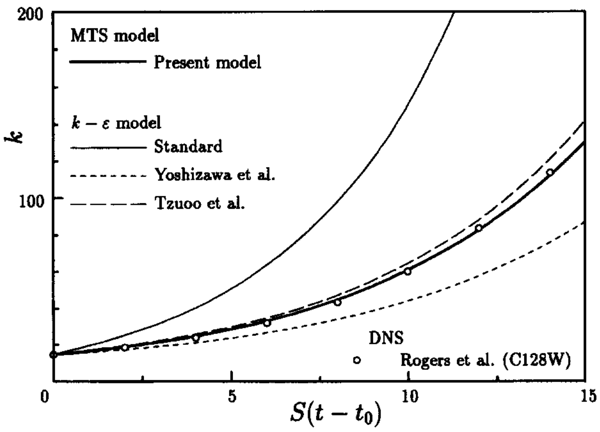

(a) Turbulent energy

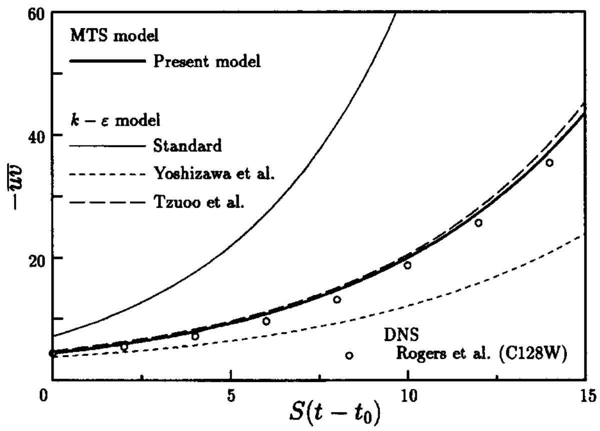

(b) Reynolds shear stress

Figure 4 Predictions of homogeneous shear flow (I) (Rogers et al. 1986; Yoshizawa et al. 1993; Tzuoo et al. 1986)

because the application of Equation 67 with the employed eddy-viscosity formulation (Equation 3) causes the negative value of k_P/k in the initial condition. The exclusion of Equation 67 removes such inconsistency, but we have no other appropriate measures to determine the initial value of k_P/k.

Figure 5 shows the comparisons of turbulence models in the flow condition of the C128U simulation of Rogers et al. (1986). Figure 5 (a) shows the turbulent energy profile, where it appears that the present model is in best agreement with DNS data. Another four models give over- or underpredictions compared to the present model and DNS data. The result of Reynolds stress evolution shown in Figure 5 (b) indicates that the present model overpredicts slightly, while the zonal model marginally underpredicts. The standard k–ε model and Duncan's (1993) MTS model predict $-\overline{uv}$ as too large, and the nonequilibrium k–ε model gives a lower prediction in the same situation.

The results of a comparison of five turbulence models with DNS data presented by Matsumoto et al. (1994) are shown in Figure 6. In this weak shear condition, the present model, zonal model, and nonequilibrium k–ε model predict the DNS data correctly. Duncan's (1993) MTS model slightly overpredicts each quantity. However, the standard k–ε model completely failed to predict this flow, and even predicted $-\overline{uv}$ to be four times greater than the DNS data at $t = t_0$. The erroneous prediction of the standard k–ε model for homogeneous shear flow seems more remarkable as the mean shear becomes weaker.

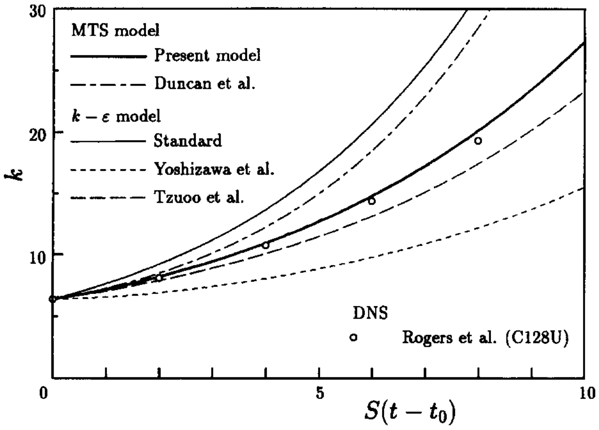

(a) Turbulent energy

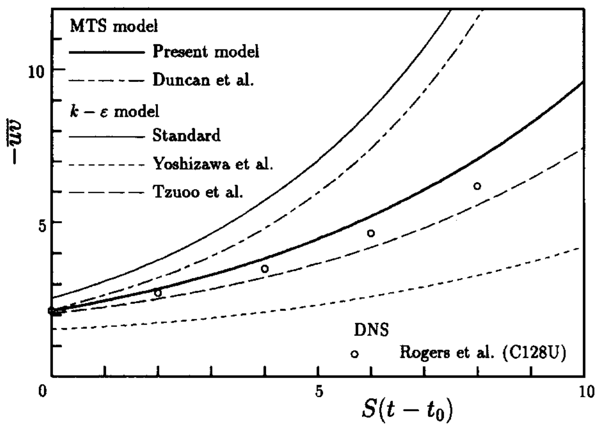

(b) Reynolds shear stress

Figure 5 Predictions of homogeneous shear flow (II) (Rogers et al. 1986; Duncan et al. 1993; Yoshizawa et al. 1993; Tzuoo et al. 1986)

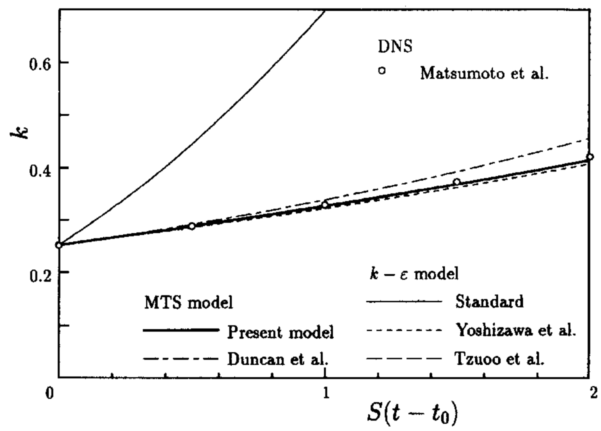

(a) Turbulent energy

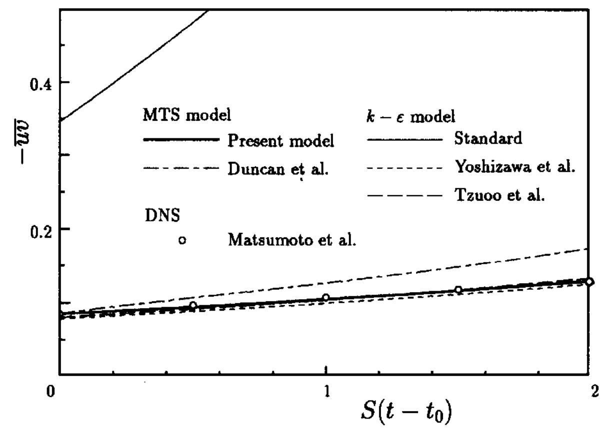

(b) Reynolds shear stress

Figure 6 Predictions of homogeneous shear flow (III) (Matsumoto et al. 1994; Duncan et al. 1993; Yoshizawa et al. 1993; Tzuoo et al. 1986)

The results in this subsection indicate that, first, the standard-type k-ε model totally fails in analyzing the homogeneous shear flow, as previously mentioned by Suzuki et al. (1993). Second, the nonequilibrium k-ε model permits a narrow range of flow conditions to obtain good results. Third, the MTS model proposed by Duncan et al (1993) overpredicts in each condition and sometimes loses the realizability constraint. The predictions of the present and zonal models have almost all proved accurate.

Fully developed channel flow

Next, we assess the model prediction of the fully developed channel flow. A comparison is made with the DNS data presented by Kim (1990) at $\mathrm{Re}_\tau = 395$. Calculations are carried out in the half-width of the channel, and symmetric boundary condition are imposed on all turbulence quantities at the center of the channel. Wall boundary conditions are represented as follows:

$$\overline{U}_w = k_{Pw} = k_{Tw} = 0 \tag{69}$$

and Equations 50 and 55 are imposed for the ε_{Pw} and ε_{Tw}, respectively. The numerical technique is based on the finite-volume method developed by Patankar (1980) and Leschziner (1982). All the results shown here, such as $\overline{U}^+ = \overline{U}/u_\tau, k^+ = k/u_\tau^2, -\overline{uv}^+ = -\overline{uv}/u_\tau^2, \varepsilon_T^+ = \varepsilon_T \nu/u_\tau^4$, are nondimensionalized by the friction velocity u_τ and the molecular viscosity ν.

Figure 7 shows the mean velocity profile of the channel flow. The present model successfully predicts the universal velocity profile in the constant stress layer: $\overline{U}^+ = 2.5 \ln y^+ + 5.0$. This is possible only is all the model constants in the present model equations satisfy the relational equations we derived in the Determination of model constants section. Agreement of the present model prediction with DNS data seems almost perfect. A profile of turbulent kinetic energy in the near-wall region is shown in Figure 8. The near-wall behavior $k \propto y^2$ is correctly

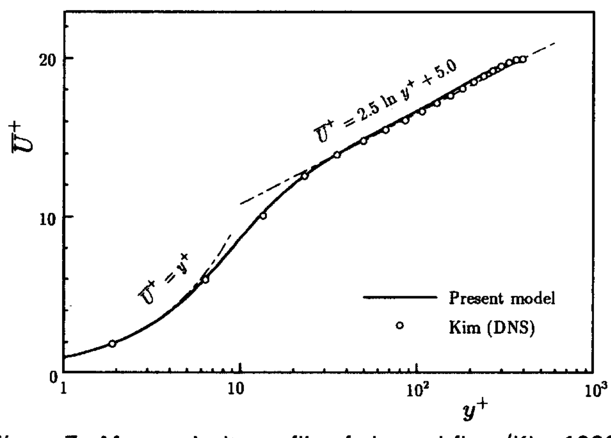

Figure 7 Mean velocity profile of channel flow (Kim 1989)

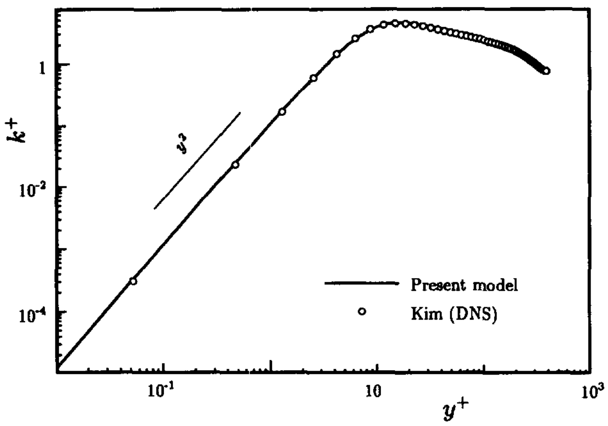

Figure 8 Near-wall behavior of turbulent energy (Kim 1989)

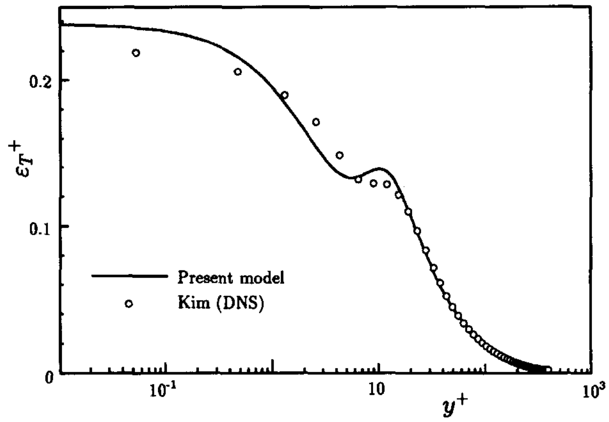

Figure 10 Dissipation rate profile of channel flow (Kim 1989)

represented by the present model, and the calculations successfully predict the DNS data. Figure 9 shows the comparison of the Reynolds shear stress prediction with DNS data in the near-wall region. The agreement of calculation results with DNS data is again almost perfect over the entire region of the channel, and the near-wall behavior $-\overline{uv} \propto y^3$ is reproduced by the correct modeling of f_ν in Equation 58. As already mentioned, the formulation f_ν is similar to the model function f_μ used in the low-Reynolds number-type k–ε model. This indicates that a similar modeling of wall turbulence is possible between the present MTS and conventional k–ε models. The dissipation rate profile is shown in Figure 10. The negative sloped distribution of ε_T near the wall was first shown by the DNS data, and this profile is also well represented by the present model.

Figure 11 presents a profile of the parameters used in the present MTS model. The relation $k_P > k_T$ indicates that the larger eddies have much turbulent kinetic energy far from the wall. But in the near-wall region, the relation is inverted because of the disappearance of energy production from the effect of a solid surface. This indicates that the dissipation process predominates over turbulence motion in the vicinity of the wall, as shown in Equation 59. This is also evident in the profile of the ratio $\varepsilon_P/\varepsilon_T$ in the same figure. In the constant stress layer, $\varepsilon_P/\varepsilon_T = 1$ holds because of the local equilibrium state, but as the wall is approached, the ratio again becomes greater. However, very near the wall, the dissipation rate ε_T is superior to the energy transfer rate ε_P, and the ratio is numerically identified with k_P/k at the wall as seen in Equation 56.

Turbulent boundary layer under various pressure gradients

Finally, we tested the present model for the turbulent boundary layer with and without pressure gradient. The numerical technique is similar to that used for the channel flow. However, information on the velocity field outside the boundary layer is in accord with the corresponding DNS and experimental data. Calculations of zero-pressure gradient (ZPG: $d\overline{P}/dx = 0$) and favorable pressure gradient (FPG: $d\overline{P}/dx < 0$) flow are made by imposing the nondimensional acceleration parameter $K = (d\overline{U}_\infty/dx)\nu/\overline{U}_\infty^2$ associated with DNS by Spalart (1986, 1988). The calculation of adverse pressure gradient (APG: $d\overline{P}/dx > 0$) flow is made by imposing a profile of static pressure coefficient $C_p \equiv 2(\overline{P} - \overline{P}_0)/\rho\overline{U}_0^2$ from the experimental data of Nagano et al. (1993) and Samuel and Joubert (1974). All results are outputted when the momentum thickness Reynolds number R_θ coincides with corresponding DNS or experimental data.

It is reported that the low-Reynolds number-type k–ε model gives a poor prediction of the APG flow, because the turbulent length-scale profile in the near-wall region is greatly affected by the pressure gradient condition (Rodi and Scheuerer 1986). It is thought that this discrepancy is because of the sensitivity of the dissipation rate equation to the pressure gradient. Under APG conditions, an approximation equation $-\overline{uv}/u_\tau^2 = 1$ is no longer supported, and the model constants optimized under the con-

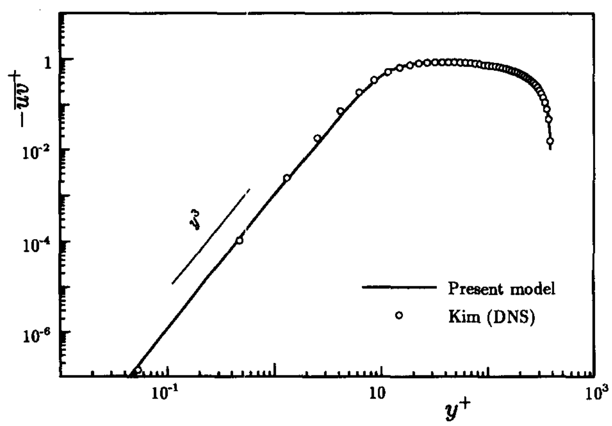

Figure 9 Near-wall behavior of Reynolds shear-stress (Kim 1989)

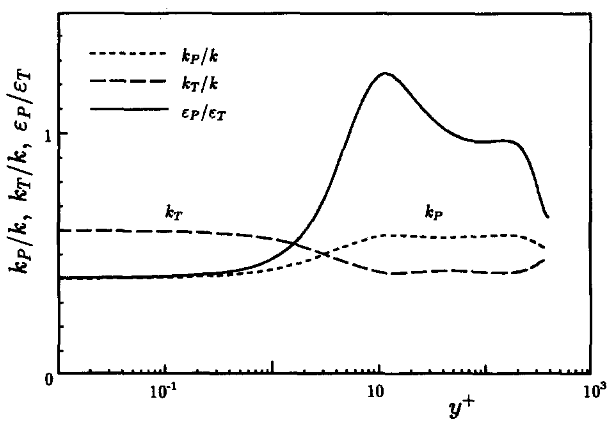

Figure 11 Variation of parameters in a channel

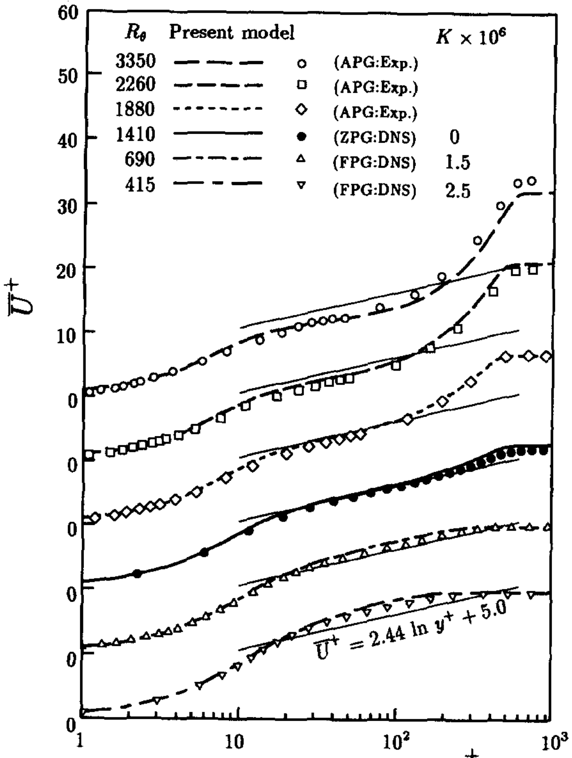

Figure 12 Mean velocity profiles of boundary-layer flow under pressure gradients

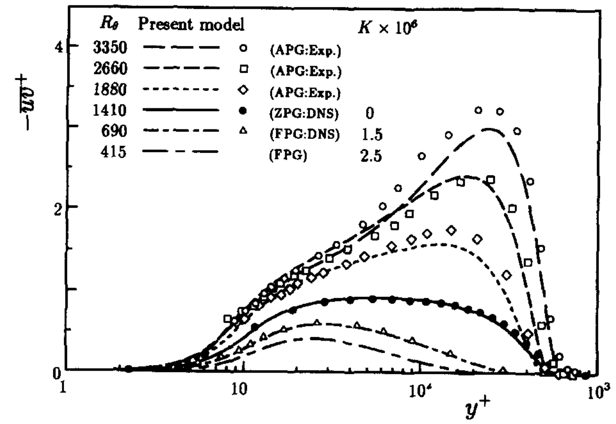

Figure 13 Reynolds shear-stress profile of boundary-layer flow under various pressure gradients

stant stress condition then become meaningless. In the present MTS model, that same error occurs in the ε_P equation, because Equation 15 is used for the determination of model constants. To resolve such a discrepancy, Hanjalić and Launder (1980) take into account the energy production from irrotational strain, which increases in proportion to the deceleration of mean velocity, with a model coefficient greater than that for the energy production term from rotational shear strain. We follow this concept and improve the production term of the present ε_P equation as follows:

$$P_{\varepsilon P} = -C_{P1}\frac{\varepsilon_P}{k_P}\overline{uv}\frac{\partial \overline{U}}{\partial y} - C'_{P1}\frac{\varepsilon_P}{k_P}(\overline{u^2} - \overline{v^2})\frac{\partial \overline{U}}{\partial x} \tag{70}$$

where $C'_{P1} = 2.8$, that is, 70% greater than C_{P1}.

Because the present model is not a nonlinear eddy-viscosity type, the normal stress difference $(\overline{u^2} - \overline{v^2})$ is calculated by an ASM similar to the calculation of the k–ε model by Nagano and Tagawa (1990). Details of the ASM we employed are described in the appendix. We restrict the use of the ASM only to the calculation of normal stresses, not shear stress, which can be obtained by the present model with high accuracy. (Developing a nonlinear MTS model is in progress to calculate flows subjected to strong pressure gradients without the aid of an ASM model.)

Figure 12 shows changes in the mean velocity profile under various pressure gradients. In the ZPG condition represented as $R_\theta = 1410$ in Figure 12, the present model produces a universal velocity profile, $\overline{U}^+ = 2.44 \ln y^+ + 5.0$, which agrees well with DNS data. The results of the FPG flows where $R_\theta = 690$ and 415 (the corresponding acceleration parameter K are 1.5×10^{-6} and 2.5×10^{-6}, respectively) reveal that the velocity profile deviate upward from the log-law of the mean velocity profile in agreement with DNS data very well.

Nagano et al. (1993) report that a downward deviation from the universal velocity profile is observed in the APG flow experiment. As shown in Figure 12, the present model well represents this profile of APG flow at $R_\theta = 1880$, 2660, and 3350. This remarkable effect is introduced by using y^* as a nondimensional distance from the wall in the model functions Equations 40 and 41 with reference to Abe et al. (1994). As the pressure gradient increases, the dissipation rate is reduced, and then y^* decreases. Hence, the model function profiles shift to a positive y-direction, thus indicating that the buffer layer becomes thicker. This is in good agreement with the experimental result.

The Reynolds shear-stress profile is shown in Figure 13. The profile on ZPG flow is almost identical to DNS data. For FPG flows, DNS data are available only at $R_\theta = 690$. The present model predicts the decrease of turbulent shear stress under the acceleration of mean velocity.

In APG flows, the constant stress layer seems to vanish entirely, and $-\overline{uv}$ profiles peak at the outer edge of the inner layer. The present model predicts this profile by improvement of the ε_P production term as Equation 70. If the production term

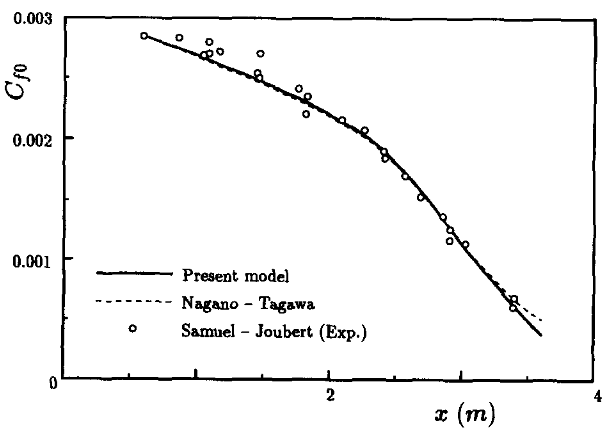

Figure 14 Skin-friction coefficient profile of adverse pressure gradient flow (Nagano and Tagawa 1990; Samuel and Joubert 1974)

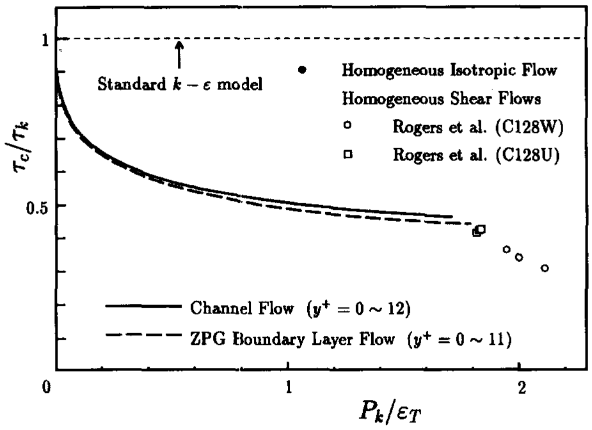

Figure 15 Variation of time-scale ratio in various fields (Rogers et al. 1986)

from irrotational strain is omitted, the velocity and the Reynolds shear-stress profile deviate from the measurements in the outer layer (not shown). In conditions of DNS by Spalart (1986), however, results of FPG flow are less changed by omission of Equation 70. Figure 14 shows the skin-friction coefficient $C_{f0} \equiv \tau_w/(\rho\bar{U}_0^2/2)$ profile according to the condition of experimental data by Samual and Joubert (1974). The present model predicts the C_{f0} profile to the farthest downstream position, similar to the $k-\varepsilon$ model by Nagano and Tagawa (1990).

These results demonstrate that the present MTS model makes fairly good predictions for the boundary-layer flow under pressure gradients. They also indicate that it shows an impressive performance for wall turbulence.

Time-scale distribution in various flows

From the results presented above, the present MTS model demonstrates versatility in analyzing the various flow fields. In predicting homogeneous shear flow, the difference in capability between the present model and the standard $k-\varepsilon$ model stands out. The strongest evidence of the superiority of the present model is the time-scale estimation.

Hereafter, we symbolize the characteristic time-scale employed in the present model as $\tau_c = k_P/\varepsilon_P$, and that of the $k-\varepsilon$ model as $\tau_k = k/\varepsilon_T$. Figure 15 is a profile of this ratio τ_c/τ_k arranged in P_k/ε_T, which is one of the parameters of the flow condition. At a position of $P_k/\varepsilon_T = 0$ as the homogeneous decaying flow, and on the solid wall, τ_c is equal to τ_k from Equations 29 and 56. The profile of τ_c/τ_k indicates that as the production rate rises, the characteristic time-scale must be reduced from τ_k, which is the standard time-scale estimation in the conventional $k-\varepsilon$ model. For the standard $k-\varepsilon$ model, the time-scale ratio cannot change from the value unity, as plotted in Figure 15. Hence, the standard $k-\varepsilon$ model overpredicts in each condition in homogeneous shear flows.

When the time-scale ratio is multiplied by the model constant C_ν, we have

$$C_\nu \frac{\tau_u}{\tau_k} = C_\nu \frac{k_P/\varepsilon_P}{k/\varepsilon_T} = C_\nu \frac{k_P}{k}\frac{\varepsilon_T}{\varepsilon_P} \tag{71}$$

which coincides with the C_μ (Equation 5). Hence, the time-scale ratio is proportional to C_μ. However, in the wall-bounded flow, τ_c/τ_k is not exactly proportional because of the influence of the model function f_ν. Rodi (1984) shows that C_μ is a function of P_k/ε_T and presents a figure of the curve. From the result of Figure 15, the C_μ profile is not expected to be a simple function of P_k/ε_T. However, a tendency for C_μ to decrease as the value of P_k/ε_T increases is verified by the computational results of the present MTS model.

Conclusions

In this paper, a new application of the multiple time-scale (MTS) turbulence model using the eddy-viscosity approximation is proposed for solving both wall and homogeneous shear flows. We model the near-wall turbulence using model functions to represent the near-wall behavior of turbulence quantities correctly, as the recent low-Reynolds number $k-\varepsilon$ model does. Furthermore, we derive relational equations among the model constants and determine these values theoretically. This work establishes a solid foundation for a low-Reynolds number MTS turbulence model using the eddy-viscosity concept.

We tested the proposed MTS model as it applies to various wall and homogeneous flows, and comparisons were made with recently available DNS and experimental data. The most notable difference between the present model and the conventional $k-\varepsilon$ model was found in prediction of homogeneous shear flow. It is concluded that this difference is not caused by a discrepancy in the eddy-viscosity approximation, but originates in the estimation of the characteristic time-scale. The profile of that time-scale in the present MTS model is shown. Furthermore, compared with some recently proposed $k-\varepsilon$ and MTS models, the proposed model demonstrates excellent versatility under various flow conditions.

Finally, we find that the profile of the characteristic time-scale estimated by the present model is qualitatively identical to the C_μ map presented by Rodi (1984). In conclusion, a turbulence model employing the eddy-viscosity concept is useful for analyzing the wall and homogeneous shear flows. However, this requires correct estimation of the characteristic time-scale suitable for various flow conditions, a requirement achieved by the present MTS turbulence model.

Acknowledgment

This research was partially supported by a Grant-in-Aid for Scientific Research in Priority Areas from the Ministry of Education, Science, and Culture of Japan (No. 05240103).

Appendix: algebraic stress model

In the calculation of boundary-layer flows with adverse pressure gradient (APG), the present model is applied with aid of the algebraic stress model (ASM) for obtaining the normal stresses in Equation 70. We used the same ASM as Nagano-Tagawa (1990) employed in their investigation.

The structural parameter $\overline{u_i u_j}/k$ is experimentally observed to be less changed in APG flow (Bradshaw 1967). Hence, the following ASM model (Rodi and Scheuerer 1983) is valid.

$$\frac{\overline{u_i u_j}}{k}(P_k - \varepsilon) = P_{ij} + \phi_{ij} + \varepsilon_{ij} \tag{A1}$$

where $P_{ij} = -(\overline{u_i u_k}\,\partial\bar{U}_j/\partial x_k + \overline{u_j u_k}\,\partial\bar{U}_i/\partial x_k)$ is the production rate of $\overline{u_i u_j}$, and the dissipation rate ε_{ij} is modeled as $\varepsilon_{ij} =$

$(2/3)\delta_{ij}\varepsilon$ $[=(2/3)\delta_{ij}\varepsilon_T]$. For the pressure–strain term ϕ_{ij}, we have chosen the isotropic production model of Launder (1985):

$$\phi_{ij} = \phi_{ij,1} + \phi_{ij,2} + \phi_{ij,w}$$

$$\phi_{ij,1} = -C_1(\varepsilon/k)(\overline{u_i u_j} - \tfrac{2}{3}\delta_{ij}k)$$

$$\phi_{ij,2} = -C_2(P_{ij} - \tfrac{2}{3}\delta_{ij}P_k) \tag{A2}$$

The wall effect for ϕ_{ij} in Equation (A2) is modeled as follows (Gibson and Launder 1978):

$$\phi_{ij,w} = \phi'_{ij,1} + \phi'_{ij,2}$$

$$\phi'_{ij,1} = C'_1(\varepsilon/k)(\overline{u_k u_m}n_k n_m \delta_{ij} - \tfrac{3}{2}\overline{u_k u_i}n_k n_j - \tfrac{3}{2}\overline{u_k u_j}n_k n_i)f$$

$$\phi'_{ij,2} = C'_2(\phi_{km,2}\, n_k n_m \delta_{ij} - \tfrac{3}{2}\phi_{ik,2} n_k n_j - \tfrac{3}{2}\phi_{jk,2} n_k n_i)f \tag{A3}$$

where $f = k^{3/2}(0.09)^{3/4}/\varepsilon y k$ is the model function, $n_i = 1$ (in the direction normal to the wall), and $n_i = 0$ (otherwise). Model constants in Equation (A2) are optimized by Younis's systematic investigation (Launder 1985) as $C_1 = 3.0$, $C_2 = 0.3$, and the constants in Equation (A3) are chosen as $C'_1 = 0.75$, $C'_2 = 0.5$ (Gibson and Younis 1986).

References

Abe, K., Kondoh, T. and Nagano, Y. 1994. A new turbulence model for predicting fluid flow and heat transfer in separating and reattaching flows—I. Flow field calculations. *Int J. Heat Mass Transfer*, **37**, 139–151

Abe, K., Kondoh, T. and Nagano, Y. 1997. On Reynolds-stress expression and near-wall scaling parameters for predicting wall and homogeneous turbulent shear flows. *Int. J. Heat Fluid Flow*, (to appear)

Abid, R. and Speziale, C. G. 1993. Predicting equilibrium states with Reynolds stress closures in channel flow and homogeneous shear flow. *Phys. Fluids A*, **5**, 1776–1782

Batchelor, G. K. and Townsend, A. A. 1948a. Decay of isotropic turbulence in the initial period. *Proc. Roy. Soc. London A*, **193**, 539–558.

Batchelor, G. K. and Townsend, A. A. 1948b. Decay of isotropic turbulence in the final period. *Proc. Royal Soc., London A*, **194**, 527–543

Bradshaw, P. 1967. The turbulence structure of equilibrium boundary layers. *J. Fluid Mech.*, **29**, 625–645

Cazalbou, J. B. and Bradshaw, P. 1993. Turbulent transport in wall-bounded flows. Evaluation of model coefficients using direct numerical simulation. *Phys. Fluids A*, **5**, 3233–3239

Chapman, D. R. and Kuhn, G. D. 1986. The limiting behaviour of turbulence near a wall. *J. Fluid Mech.*, **170**, 265–292

Coleman, G. N. and Mansour, N. N. 1993. Simulation and modeling of homogeneous compressible turbulence under isotropic mean compression. In *Turbulent Shear Flows 8*. F. Durst, R. Friedrich, B. E. Launder, F. W. Schmidt, U. Schumann and J. H. Whitelaw (eds.), Springer-Verlag, Heidelberg, Germany 269–282

Comte-Bellot, G. and Corrsin, S. 1966. The use of a contraction to improve the isotropy of grid-generated turbulence. *J. Fluid Mech.*, **25**, 657–682

Corrsin, S. 1951. The decay of isotropic temperature fluctuations in an isotropic turbulence. *J. Aeronaut. Sci.*, **18**, 417–423

Duncan, B. S., Liou, W. W. and Shih, T. H. 1993. A multiple-scale turbulence model for incompressible flow. *NASA TM*-106113

Gatski, T. B. and Speziale, C. G. 1993. On explicit algebraic stress models for complex turbulent flows. *J. Fluid Mech.*, **254**, 59–78

Gibson, M. M. and Launder, B. E. 1978. Ground effects on pressure fluctuations in the atmospheric boundary layer. *J. Fluid Mech.*, **86**, 491–511

Gibson, M. M. and Younis, B. A. 1986. Calculation of boundary layers with sudden transverse strain. *J. Fluids Eng.*, **108**, 470–475

Hanjalić, K. 1994. Advanced turbulence closure models: A view of current status and future prospects. *Int. J. Heat Fluid Flow*, **15**, 178–203

Hanjalić, K. and Launder, B. E. 1980. Sensitizing the dissipation equation to irrotational strains. *J. Fluids Eng.*, **102**, 34–40

Hanjalić, K., Launder, B. E. and Schiestel, R. 1980. Multiple-time-scale concepts in turbulent transport modeling. In *Turbulent Shear Flows 2*, L. J. S. Bradbury, F. Durst, B. E. Launder, F. W. Schmidt and J. H. Whitelaw (eds.), Springer, Berlin, 36–49

Iida, O. and Kasagi, N. 1993. Direct numerical simulation of homogeneous isotropic turbulence with heat transport (Prandtl number effects). *Trans. JSME*, B, **59**, 3359–3364

Kim, J. 1990. Collaborative testing of turbulence models. Data Disk No. 4

Kim, S. W. 1991. Calculation of divergent channel flows with a multiple-time-scale turbulence model. *AIAA J.*, **29**, 547–554

Kim, S. W. and Benson T. J. 1992. Calculation of a circular jet in crossflow with a multiple-time-scale turbulence model. *Int. J. Heat Mass Transfer*, **35**, 2357–2365

Kim, S. W. and Chen, C. P. 1989. A multiple-time-scale turbulence model based on variable partitioning of the turbulent kinetic energy spectrum. *Numer. Heat Transfer B*, **16**, 193–211

Launder, B. E. 1985. Progress and prospects in phenomenological turbulence models. *Theoretical Approaches to Turbulence*, D. L. Dwoyer, M. Y. Hussaini and R. G. Voigt (eds.), Springer-Verlag, Berlin, 155–186

Leschziner, M. A. 1982. *An Introduction and Guide to the Computer Code PASSABLE*. UMIST Dept. of Mech. Eng. Rep. TF/11/82

Liou. W. W. 1992. Modeling of turbulent shear flows. NASA TM-105834, 67–75

Matsumoto, A., Nagano, Y. and Tsuji, T. 1994. Effects of mean shear on homogeneous turbulence (turbulence statistics and turbulence models). *Trans. JSME, B*, **60**, 573, 1653–1660

Michelassi, V. 1993. Adverse pressure gradient flow computation by two-equation turbulence models. In *Engineering Turbulence Modeling and Experiments 2*, W. Rodi and F. Martelli (eds.), Elsevier, New York, 123–132

Myong, H. K. and Kasagi, N. 1990. A new approach to the improvement of k–ε turbulence model for wall-bounded shear flows. *JSME Int. J. II*, **33**, 63–72

Myong, H. K., Kasagi, N. and Hirata, M. 1989. Numerical prediction of turbulent pipe flow heat transfer for various Prandtl number fluids with the improved k–ε turbulence model. *JSME Int. J. II*, **32**, 613–622

Nagano, Y. and Hishida, M. 1987. Improved form of the k–ε model for wall turbulent shear flows. *J. Fluids Eng.*, **109**, 156–160

Nagano, Y. and Shimada, M. 1993. Modeling the dissipation-rate equation for two-equation turbulence model. *Proc. 9th Symposium on Turbulent Shear Flows*, Kyoto, Japan, Vol. 3, 23.2.1–23.2.6

Nagano, Y. and Shimada, M. 1995. Rigorous modeling of dissipation-rate equation using direct simulation. *JSME Int. J. B.*, **38**, 51–59

Nagano, Y. and Tagawa; M. 1990. An improved k–ε model for boundary layer flows. *J. Fluids Eng.*, **112**, 33–39

Nagano, Y., Tagawa, M. and Tsuji, T. 1993. Effects of adverse pressure gradients on mean flows and turbulence statistics in a boundary layer. In *Turbulent Shear Flows* 8, F. Durst, R. Friedrich, B. E. Launder, F. W. Schmidt, U. Schumann and J. H. Whitelaw (eds.), Springer-Verlag, Berlin, Heidelberg, 7–21

Patankar, S. V. 1980. *Numerical Heat Transfer and Fluid Flow*. Hemisphere, Bristol, PA

Rodi, W. 1984. *Turbulence Models and Their Application in Hydraulics*. IAHR, Delft, The Netherlands

Rodi, W. and Mansour, N. N. 1993. Low-Reynolds number k–ε modeling with the aid of direct simulation data. *J. Fluid Mech.*, **250**, 509–529

Rodi, W. and Scheuerer, G. 1983. Calculation of curved shear layers with two-equation turbulence models. *Phys. Fluids*, **26**, 1422–1436

Rodi, W. and Scheuerer, G. 1986. Scrutinizing the k–ε turbulence model under adverse pressure gradient conditions. *J. Fluids Eng.*, **108**, 174–179

Rogers, M. M., Moin, P. and Reynolds, W. C. 1986. The structure and modeling of the hydrodynamics and passive scalar field in homogeneous turbulent shear flow. NASA NCC-2-15

Samuel, A. E. and Joubert, P. N. 1974. A boundary layer developing in an increasingly adverse pressure gradient. *J. Fluid Mech.*, **66**, 481–505

Schiestel, R. 1987. Multiple time-scale modeling of turbulent flows in on point closures. *Phys. Fluids*, **30**, 722–731

Spalart, P. R. 1986. Numerical study of sink-flow boundary layers. *J. Fluid Mech.*, **172**, 307–328

Spalart, P. R. 1988. Direct simulation of a turbulent boundary layer up to $R_\theta = 1410$. *J. Fluid Mech.*, **187**, 61–98

Suzuki, N., Matsumoto, A., Nagano, Y., Tagawa, M. 1993. Anisotropy of heat transport and its modeling in homogeneous turbulent flow. *Heat Trans, Japan Res.* **22**, 325–339

Tzuoo, K. L., Ferziger, J. H. and Kline, S. J. 1986. Zonal models of turbulence and their application to free shear flows. TF-27, Standford University, Standford, CA

Yoshizawa, A. and Nishizima, S. 1993. A nonequilibrium representation of the turbulent viscosity based on a two-scale turbulence theory. *Phys. Fluids A*, **5**, 3302–3304

Youssef, M. S., Nagano, Y. and Tagawa, M. 1992. A two-equation heat transfer model for predicting turbulent thermal fields under arbitrary wall thermal conditions. *Int. J. Heat Mass Transfer*, **35**, 3095–3104